Charmed nuclei within a microscopic many-body approach

I. Vidaña,[1] A. Ramos,[2] and C. E. Jiménez-Tejero[3]

[1]*Istituto Nazionale di Fisica Nucleare, Sezione di Catania, Dipartimento di Fisica "Ettore Majorana", Università di Catania, Via Santa Sofia 64, I-95123 Catania, Italia*

[2]*Departament de Física Quàntica i Astrofísica and Institut de Ciències del Cosmos (ICCUB), Facultat de Física, Universitat de Barcelona, Martí i Franquès 1, E-08028 Barcelona, Spain*

[3]*Barcelona Center for Subsurface Imaging, Institute of Marine Sciences, Spanish Research Council, Passeig Marítim de la Barceloneta 37, E-08003 Barcelona, Spain*

(Received 28 January 2019; revised manuscript received 21 March 2019; published 23 April 2019)

Single-particle energies of the Λ_c charmed baryon are obtained in several nuclei from the relevant self-energy constructed within the framework of a perturbative many-body approach. Results are presented for a charmed baryon-nucleon (Y_cN) potential based on a SU(4) extension of the meson-exchange hyperon-nucleon potential $\tilde{A}$ of the Jülich group. Three different models (A, B, and C) of this interaction, which differ only on the values of the couplings of the scalar σ meson with the charmed baryons, are considered. Phase shifts, scattering lengths, and effective ranges are computed for the three models and compared with those predicted by the Y_cN interaction derived by Haidenbauer and Krein [Eur. Phys. A **54**, 199 (2018)] from the extrapolation to the physical pion mass of recent results of the HAL QCD Collaboration. Qualitative agreement is found for two of the models (B and C) considered. Our results for Λ_c nuclei are compatible with those obtained by other authors based on different models and methods. We find a small spin-orbit splitting of the p-, d-, and f-wave states as in the case of single Λ hypernuclei. The level spacing of Λ_c single-particle energies is found to be smaller than that of the corresponding one for hypernuclei. The role of the Coulomb potential and the effect of the coupling of the Λ_cN and Σ_cN channels on the single-particle properties of Λ_c nuclei are also analyzed. Our results show that, despite the Coulomb repulsion between the Λ_c and the protons, even the less attractive one of our Y_cN models (model C) is able to bind the Λ_c in all the nuclei considered. The effect of the Λ_cN-Σ_cN coupling is found to be almost negligible due to the large mass difference of the Λ_c and Σ_c baryons.

DOI: 10.1103/PhysRevC.99.045208

I. INTRODUCTION

Soon after the discovery of charmed hadrons [1–6], the possible existence of charmed nuclei (bound systems composed of nucleons and charmed baryons) was proposed in analogy with hypernuclei (see, e.g., Refs. [7–11]). This possibility motivated several authors to study the properties of these systems within different theoretical approaches, predicting a rich spectrum and a wide range of atomic numbers [12–18]. Production mechanisms of charmed nuclei by means of *charm exchange* or *associate charm production* reactions, analogous to the ones widely used in hypernuclear physics, were also proposed [19,20]. However, the experimental production of charmed nuclei is difficult and, up to now, only three ambiguous candidates have been reported by an emulsion experiment carried out in Dubna in the mid 1970s [21–25]. Experimental difficulties arise mainly from (i) the kinematics of the production reactions: charmed particles are formed with large momentum making their capture by a target-nucleus improbable; and (ii) the short lifetimes of D-meson beams, which makes it necessary to place the target as close as possible to the D-meson production point. Such difficulties will be hopefully overcome at the future GSI-FAIR (Gesellschaft für Schwerionenforschung–Facility for Antiproton and Ion Research) and JPARC (Japan Proton Accelerator Research Complex) facilities [26,27]. The production of charmed particles in these facilities will be sufficiently large to make the study of charmed nuclei possible. Studies of $\bar{p}$ reactions in nuclei under the conditions of the $\overline{\text{P}}$ANDA experiment predict forward differential cross sections for the formation of Λ_c hypernuclei in the range of a few μb/sr [28]. These future prospects have injected a renewed interest in this line of research [29]. In the last few years, theoretical estimations of the charmed baryon properties in nuclear matter and finite nuclei have been revisited using the quark-meson coupling model [30–33], a relativistic mean-field approach [34], effective Lagrangians satisfying the heavy quark, chiral and hidden local symmetries [35], the quark cluster model [36], and a single-folding potential employing a lattice QCD (LQCD) simulation of the Λ_cN interaction [37]. An extrapolation to the physical pion mass of the former LQCD Λ_cN interaction has recently become available [38].

In this work we study the single-particle properties of the Λ_c charmed baryon in several nuclei using a microscopic many-body approach. Our starting point is a nuclear matter G matrix derived from a bare charmed baryon-nucleon (Y_cN, $Y_c = \Lambda_c$ and Σ_c) potential based on a SU(4) extension of the hyperon-nucleon (YN) potential $\tilde{A}$ of the Jülich group [39]. This G matrix is used to calculate the self-energy of the Λ_c in

the finite nucleus including corrections up to the second order. Solving the Schrödinger equation with this self-energy we are able to determine the single-particle energies and the wave function of the bound Λ_c. Our approach also provides the real and imaginary parts of the Λ_c optical potential at positive energies and therefore allows one to study the Λ_c-nucleus scattering properties. This method was already used to study the properties of the nucleon [40], the Δ isobar [41], and the Λ and Σ hyperons [42–45] in finite nuclei.

The paper is organized in the following way. In Sec. II we present our model for the Y_cN interaction. The method to obtain the Λ_c single-particle properties in finite nuclei is briefly described in Sec. III. Results for a variety of Λ_c nuclei are shown in Sec. IV. Finally, a brief summary and some concluding remarks are given in Sec. V.

II. THE Y_cN INTERACTION

Our model for the Y_cN interaction is based on a generalization of the meson exchange YN potential $\tilde{A}$ of the Jülich group [39]. In analogy with that model, we describe the three different channels, $\Lambda_cN \to \Lambda_cN$, $\Sigma_cN \to \Sigma_cN$, and $\Lambda_cN \leftrightarrow \Sigma_cN$, only as the sum of single scalar, pseudoscalar, and vector meson exchange potentials shown in Fig. 1. As in the YN Jülich potential, the exchange of the effective scalar σ meson parametrizes the contribution of correlated 2π exchange. The basic elements of our model are the baryon-baryon-pseudoscalar (BBP) and the baryon-baryon-vector (BBV) vertices described, respectively, by the Lagrangian densities

$$\begin{aligned}\mathcal{L}_{\rm BBP} &= g_{NN\pi}(N^\dagger\vec{\tau}N)\cdot\vec{\pi} + g_{\Lambda_c\Sigma_c\pi}[\vec{\Sigma}_c^\dagger\cdot\vec{\pi}\,\Lambda_c + \Lambda_c^\dagger\vec{\Sigma}_c\cdot\vec{\pi}] \\ &\quad - ig_{\Sigma_c\Sigma_c\pi}(\vec{\Sigma}_c^\dagger\times\vec{\Sigma}_c)\cdot\vec{\pi} + g_{N\Lambda_cD}[(N^\dagger D)\Lambda_c \\ &\quad + \Lambda_c^\dagger(D^\dagger N)] + g_{N\Sigma_cD}[(N^\dagger\vec{\tau}D)\cdot\vec{\Sigma}_c + \vec{\Sigma}_c^\dagger(D^\dagger\vec{\tau}N)]\end{aligned}$$

and

$$\begin{aligned}\mathcal{L}_{\rm BBV} &= g_{NN\rho}(N^\dagger\vec{\tau}N)\cdot\vec{\rho} + g_{\Lambda_c\Sigma_c\rho}[\vec{\Sigma}_c^\dagger\cdot\vec{\rho}\Lambda_c + \Lambda_c^\dagger\vec{\Sigma}_c\cdot\vec{\rho}] \\ &\quad - ig_{\Sigma_c\Sigma_c\rho}(\vec{\Sigma}_c^\dagger\times\vec{\Sigma}_c)\cdot\vec{\rho} + g_{N\Lambda_cD^*}[(N^\dagger D^*)\Lambda_c \\ &\quad + \Lambda_c^\dagger(D^{*\dagger}N)] + g_{N\Sigma_cD^*}[(N^\dagger\vec{\tau}D^*)\cdot\vec{\Sigma}_c \\ &\quad + \vec{\Sigma}_c^\dagger(D^{*\dagger}\vec{\tau}N)] + g_{NN\omega}N^\dagger N\omega \\ &\quad + g_{\Lambda_c\Lambda_c\omega}\Lambda_c^\dagger\Lambda_c\omega + g_{\Sigma_c\Sigma_c\omega}\vec{\Sigma}_c^\dagger\cdot\vec{\Sigma}_c\omega.\end{aligned}$$

We note that the isospin structure of these vertices is the same as that of their analogous strange ones. Similarly to the Jülich YN interaction, which is itself based on the Bonn NN one, the Y_cN model presented here also neglects the contribution of the η and η' mesons.

We use the SU(4) symmetry to derive the relations between the different coupling constants. Note, however, that this symmetry is strongly broken due to the use of the different physical masses of the various baryons and mesons and that we employ it rather as a mathematical tool to get a handle on the various couplings of our model. In particular, we are dealing with $J^P = \frac{1}{2}^+$ baryons and $J^P = 0^-$ and 1^- mesons belonging to $20'$- and 15-plet irreducible representations of SU(4), respectively. Because the baryon current can be

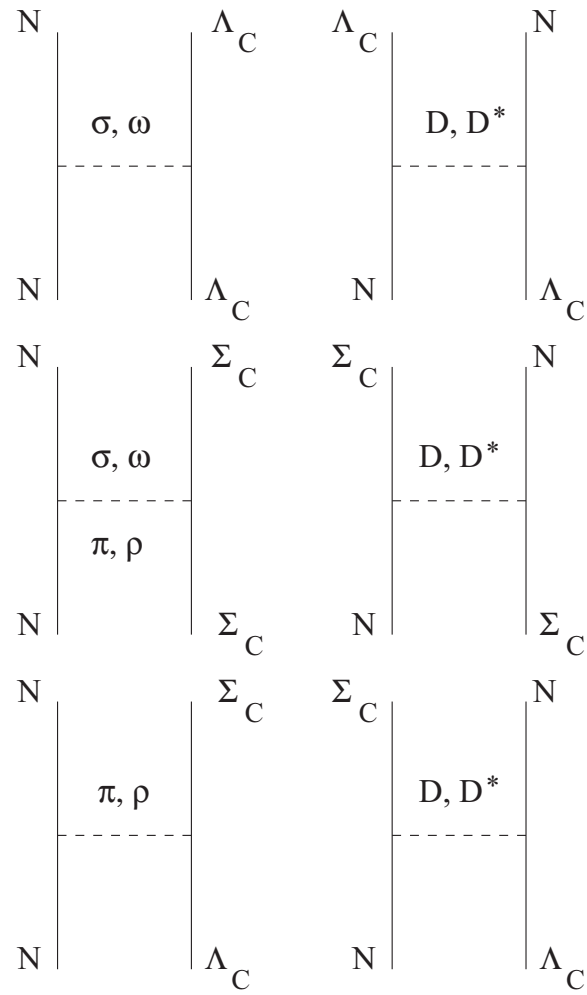

FIG. 1. Single-meson exchange contributions included in our model for the Y_cN interaction.

reduced according to

$$\mathbf{20'}\otimes\overline{\mathbf{20'}} = \mathbf{1}\oplus\mathbf{15_1}\oplus\mathbf{15_2}\oplus\mathbf{20''}\oplus\mathbf{45}\oplus\overline{\mathbf{45}}\oplus\mathbf{84}\oplus\mathbf{175}, \tag{1}$$

there are two ways to obtain an SU(4) scalar for the coupling $\mathbf{20'}\otimes\overline{\mathbf{20'}}\otimes\mathbf{15}$ because the baryon current contains two distinct 15-plet representations, $\mathbf{15_1}$ and $\mathbf{15_2}$. They couple to the meson 15 plets with strengh g_{15_1} and g_{15_2}, respectively. It is quite straightforward to relate these two couplings to the couplings g_D and g_F of the usual symmetric ("D-coupling") and antisymmetric ("F-coupling") octet representations of the baryon current in SU(3). They read

$$\begin{aligned}g_{15_1} &= \frac{1}{4}(7g_D + \sqrt{5}g_F) = \sqrt{\frac{10}{3}}g_8(7-4\alpha), \\ g_{15_2} &= \sqrt{\frac{3}{20}}(\sqrt{5}g_D - 5g_F) = \sqrt{40}g_8(1-4\alpha),\end{aligned} \tag{2}$$

where in the last step we have written g_D and g_F in terms of the conventional SU(3) octet strength coupling g_8 and the

so-called $F/(F+D)$ ratio α:

$$g_D = \frac{40}{\sqrt{30}} g_8(1-\alpha), \quad g_F = 4\sqrt{6} g_8 \alpha. \tag{3}$$

Let us first consider the coupling of the baryon current to the pseudoscalar mesons. The relations between all the relevant BBP coupling constants can easily be obtained by using SU(4) Clebsch-Gordan coefficients [46] and the above relations. They read

$$\begin{aligned} g_{\Lambda_c\Sigma_c\pi} &= \frac{2}{\sqrt{3}} g_{NN\pi}(1-\alpha_p), \\ g_{\Sigma_c\Sigma_c\pi} &= 2\, g_{NN\pi}\alpha_p, \\ g_{N\Lambda_c D} &= -\frac{1}{\sqrt{3}} g_{NN\pi}(1+2\alpha_p), \\ g_{N\Sigma_c D} &= g_{NN\pi}(1-2\alpha_p), \end{aligned} \tag{4}$$

where we have added the subindex p to the ratio α to specify that this is the ratio for the coupling of baryons with the pseudoscalar mesons and to distinguish it from that for the vector ones used below.

Similarly, the corresponding relations for the BBV couplings can be obtained by simply making the replacements $\pi \to \rho$, $D \to D^*$, and $\alpha_p \to \alpha_v$ in the above expressions. In addition, the couplings to the ω meson are

$$\begin{aligned} g_{NN\omega} &= g_{NN\rho}(4\alpha_v - 1), \\ g_{\Lambda_c\Lambda_c\omega} &= \frac{g_{NN\rho}}{9}(6\alpha_v + 3), \\ g_{\Sigma_c\Sigma_c\omega} &= g_{NN\rho}(2\alpha_v - 1), \end{aligned} \tag{5}$$

where we have assumed that the physical ω meson results from the ideal mixing of the mathematical members of the 15-plet ω_8 and ω_1.

The relations for the tensor coupling constants $f_{\rm BBM}$ can be obtained by applying the corresponding SU(4) relations to the "magnetic" coupling $G_{\rm BBM} = g_{\rm BBM} + f_{\rm BBM}$. Thus, in the above relations g_v has to be replaced simply by G_v and α_v by α_t.

Regarding the couplings of the scalar σ meson with the charmed baryons, we note that this meson is not a member of any SU(4) multiplet and, therefore, it is not possible to obtain these couplings by invoking the SU(4) symmetry as we did for the couplings with the pseudoscalar and vector mesons. This leaves us certain freedom to chose the values of the couplings $g_{\Lambda_c\Lambda_c\sigma}$ and $g_{\Sigma_c\Sigma_c\sigma}$. To explore the sensitivity of our results to these couplings, in this work we consider three different sets of values that, together with the pseudoscalar and vector meson couplings, define three models for the Y_cN interaction. From now on we refer to these models simply as A, B, and C. In model A the couplings of the σ meson with the charmed baryons are assumed to be equal to those with the Λ and Σ hyperons, and their values are taken from the original YN potential $\tilde{A}$ of the Jülich group [39]. In models B and C these couplings are reduced by 15 and 20%, respectively, with respect to model A. The coupling $g_{NN\sigma}$ has been taken, for the three models, to be equal to that of the Jülich $\tilde{A}$ YN potential.

Using the values $\alpha_P = 0.4$, $\alpha_v = 1$, and $\alpha_t = 0.4$ given in Ref. [39], we obtain the couplings reported in Table I, where we also show the cutoff masses $\Lambda_{\rm BBM}$ of the monopole form factors of the different vertices. We note that, to describe the nucleon-nucleon data quantitatively, the coupling $g_{NN\omega}$ in the Jülich $\tilde{A}$ YN model was increased by a factor of 1.626 with respect to its SU(3) value, $g_{NN\omega} = 3g_{NN\rho}$, thereby accounting for missing short-range correlations in an effective way. In the present work, we apply the same increasing factor to the $g_{\Lambda_c\Lambda_c\omega}$ and $g_{\Sigma_c\Sigma_c\omega}$ coupling constants of Eq. (5). We also note that the relation of these coupling constants to $g_{NN\rho}$ is a factor of 2 smaller than that obtained in the SU(3) sector, while the relations in Eq. (4), involving charmed baryons and the π, ρ, D, and D^* mesons, are the same as those involving their counterparts in the strange sector.

TABLE I. Baryon-baryon-meson coupling constants $g_{\rm BBM}$ and $f_{\rm BBM}$ and cutoff masses $\Lambda_{\rm BBM}$ for the models A, B, and C of the Y_cN interaction constructed and used in this work.

Model	Vertex	$g_{\rm BBM}/\sqrt{4\pi}$	$f_{\rm BBM}/\sqrt{4\pi}$	$\Lambda_{\rm BBM}$ (GeV)
A, B, C	$NN\pi$	3.795	–	1.3
A, B, C	$\Lambda_c\Sigma_c\pi$	3.067	–	1.4
A, B, C	$\Sigma_c\Sigma_c\pi$	2.277	–	1.2
A, B, C	$N\Lambda_c D$	−3.506	–	2.5
A, B, C	$N\Sigma_c D$	1.518	–	2.5
A, B, C	$NN\rho$	0.917	5.591	1.4
A, B, C	$\Lambda_c\Sigma_c\rho$	0.000	4.509	1.16
A, B, C	$\Sigma_c\Sigma_c\rho$	1.834	3.372	1.41
A, B, C	$NN\omega$	4.472	0.000	1.5
A, B, C	$\Lambda_c\Lambda_c\omega$	1.490	2.758	2.0
A, B, C	$\Sigma_c\Sigma_c\omega$	1.490	−2.907	2.0
A, B, C	$N\Lambda_c D^*$	−1.588	−5.175	2.5
A, B, C	$N\Sigma_c D^*$	−0.917	2.219	2.5
A, B,C	$NN\sigma$	2.385	–	1.7
A	$\Lambda_c\Lambda_c\sigma$	2.138	–	1.0
A	$\Sigma_c\Sigma_c\sigma$ $(I=1/2)$	3.061	–	1.0
A	$\Sigma_c\Sigma_c\sigma$ $(I=3/2)$	3.102	–	1.12
B	$\Lambda_c\Lambda_c\sigma$	1.817	–	1.0
B	$\Sigma_c\Sigma_c\sigma$ $(I=1/2)$	2.601	–	1.0
B	$\Sigma_c\Sigma_c\sigma$ $(I=3/2)$	2.636	–	1.12
C	$\Lambda_c\Lambda_c\sigma$	1.710	–	1.0
C	$\Sigma_c\Sigma_c\sigma$ $(I=1/2)$	2.448	–	1.0
C	$\Sigma_c\Sigma_c\sigma$ $(I=3/2)$	2.481	–	1.12

The three Y_cN interaction models have then been used to solve the coupled-channel (Λ_cN, Σ_cN) Lipmann-Schwinger equation to obtain several scattering observables from the corresponding scattering amplitudes. The Λ_cN phase shifts in the $^1S_0$ and $^3S_1$ partial waves are shown as functions of the center-of-mass kinetic energy in Fig. 2 for the three models. The extrapolation to the physical pion mass of the recent results of the HAL QCD Collaboration [37] made by Haidenbauer and Krein in Ref. [38] is shown by the thick green band for comparison. One can clearly see from the phase shifts that model A predicts a more attractive Λ_cN interaction in the $^1S_0$ and $^3S_1$ partial waves than the one derived in Ref. [38]. The reduction of the $g_{\Lambda_c\Lambda_c\sigma}$ and $g_{\Sigma_c\Sigma_c\sigma}$ couplings in models B and C leads to a reduction of attraction in these

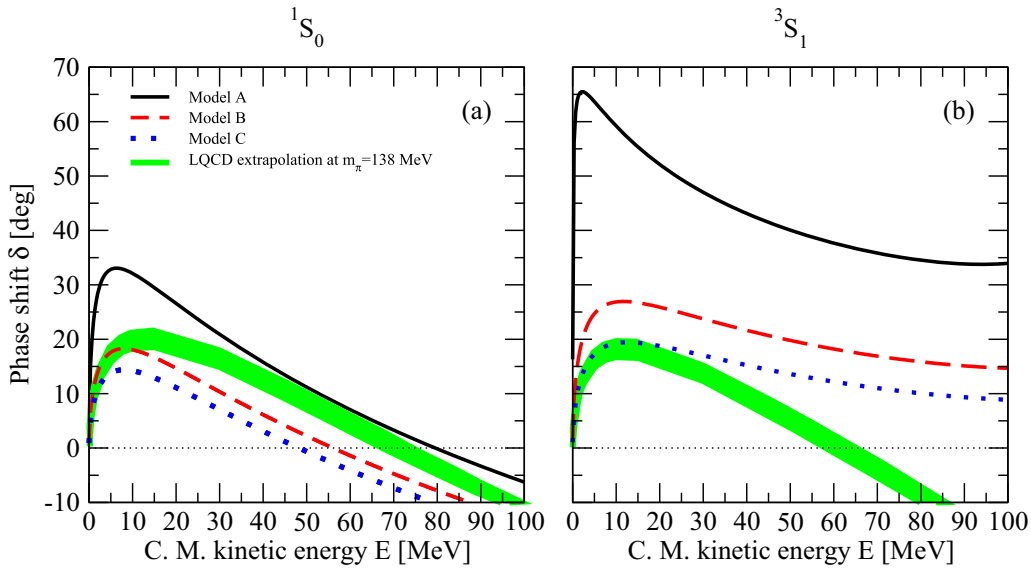

FIG. 2. $^1S_0$ [panel (a)] and $^3S_1$ [panel (b)] $\Lambda_c N$ phase shifts as a function of the center-of-mass kinetic energy. Results are shown for models A, B, and C. The thick band shows the extrapolation to the physical pion mass of the recent results of the HAL QCD Collaboration [37] made by Haidenbauer and Krein in Ref. [38].

two partial waves which translates into a qualitatively better agreement between the phase shifts predicted by these two models and those obtained from the interaction of Ref. [38], particularly in the low-energy region. Note that the interaction derived in Ref. [38] predicts similar phase shifts for both partial waves since the corresponding $^1S_0$ and $^3S_1$ potentials are almost identical, a feature already noted by the HAL QCD Collaboration at different values of the pion mass (see Ref. [37]) that seems to persist when extrapolating the lattice results to the physical point. This, however, is not the case for our models A, B, and C, which predict more overall attraction in the $^3S_1$ partial wave. This can also be seen, for example, in Fig. 3 where we show the diagonal $^1S_0$ and $^3S_1$ matrix elements of the $\Lambda_c N \to \Lambda_c N$ channel in momentum space.

For completeness, we report in Table II the singlet and triplet $\Lambda_c N$ scattering lengths and the effective range predicted by the three models. The results obtained by Haidenbauer and Krein in Ref. [38] are shown for comparison in the last column of the table. There is a good agreement between model C and the results of Ref. [38] for both scattering lengths. However, is it pointed out in Ref. [38] that the scattering lengths at the physical pion mass could in fact be as larger as -1.3 fm if the uncertainty of ± 0.2 fm, given by the HAL QCD Collaboration for their result at $m_\pi = 410$ MeV, is

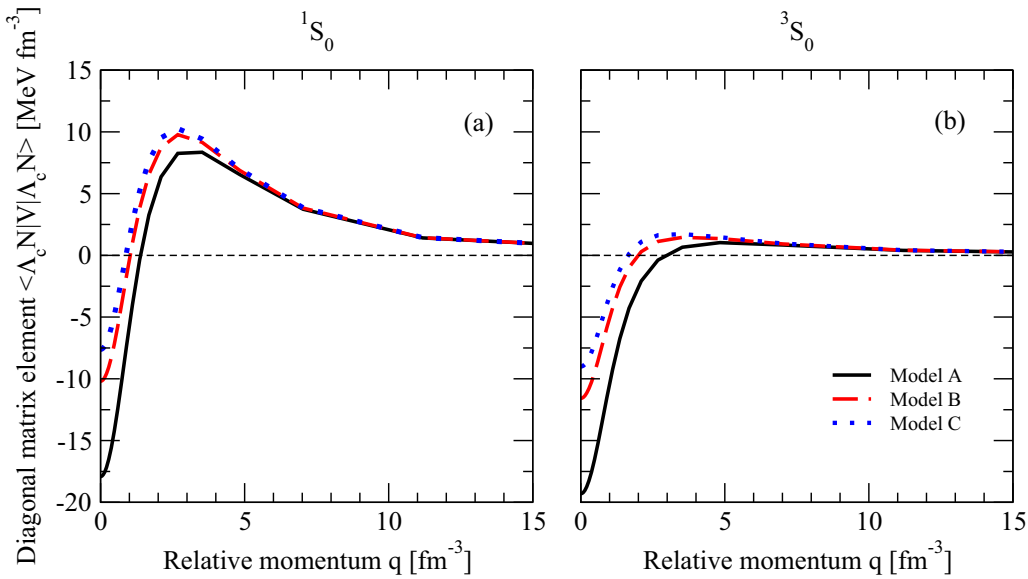

FIG. 3. $^1S_0$ [panel (a)] and $^3S_1$ [panel (b)] $\Lambda_c N \to \Lambda_c N$ diagonal matrix elements as a function of the relative momentum q. Results are shown for models A, B, and C.

TABLE II. Singlet and triplet $\Lambda_c N$ scattering lengths and effective ranges predicted by the models A, B, and C. The results of the extrapolation to the physical pion mass of the recent results of the HAL QCD Collaboration [37] made by Haidenbauer and Krein in Ref. [38] are shown in the last column. Units are given in fm.

	Model A	Model B	Model C	Ref. [38]
a_s	−2.60	−1.11	−0.84	−0.85 . . . − 1.00
r_s	2.86	4.40	5.38	2.88 . . . 2.61
a_t	−15.87	−1.52	−0.99	−0.81 . . . − 0.98
r_t	1.64	2.79	3.63	3.50 . . . 3.15

combined with the observation that variations in the scattering lengths of ±0.05 fm at this value of the pion mass amount to differences of about ±0.1 fm at $m_\pi = 138$ MeV. In this case, the prediction of model B would be in better agreement with the result of Haidenbauer and Krein than model C. Model A predicts a singlet effective range compatible with that obtained in Ref. [38], although it predicts a smaller triplet one. On the other hand, models B and C give a singlet effective range larger than that of Ref. [38] but their agreement is qualitatively better for the triplet one.

III. Λ_c SINGLE-PARTICLE PROPERTIES IN FINITE NUCLEI

Here we briefly describe a method to obtain the Λ_c single-particle energies in a finite nucleus using an effective in-medium Y_cN interaction derived from the bare Y_cN potential presented in the previous section. The starting point of this method is the calculation of all the Y_cN G matrices, which describe the interaction between a charmed baryon ($Y_c = \Lambda_c$ and Σ_c) and a nucleon in infinite nuclear matter. The G matrices are obtained by solving the coupled-channel Bethe-Goldstone equation, written schematically as

$$G_{Y_cN\to Y_c'N'}(\omega) = V_{Y_cN\to Y_c'N'} + \sum_{Y_c''N''} V_{Y_cN\to Y_c''N''} \times \frac{Q_{Y_c''N''}}{\omega - \epsilon_{Y_c''} - \epsilon_{N''} + i\eta} G_{Y_c''N''\to Y_c'N'}(\omega), \quad (6)$$

where V is the bare Y_cN potential derived in the previous section, Q is the Pauli operator that prevents the nucleon in the intermediate state $Y_c''N''$ from being scattered below the Fermi momentum k_{F_N}, and ω is the nuclear matter starting energy that corresponds to the sum of the masses and the nonrelativistic energies of the interacting charmed baryon and nucleon. We note that the Bethe-Goldstone equation has been solved in momentum space including partial waves up to a maximum value of the total angular momentum $J = 4$. We note also here that the so-called discontinuous prescription has been adopted; i.e., the single-particle energies $\epsilon_{Y_c''}$ and $\epsilon_{N''}$ in the denominator of Eq. (6) are simply taken as the sum of the nonrelativistic kinetic energy plus the mass of the corresponding baryon.

The finite nucleus Y_cN G matrix, $G_{\rm FN}$, can be obtained, in principle, by solving the Bethe-Goldstone equation directly in the finite nucleus [47,48]. The Bethe-Goldstone equation

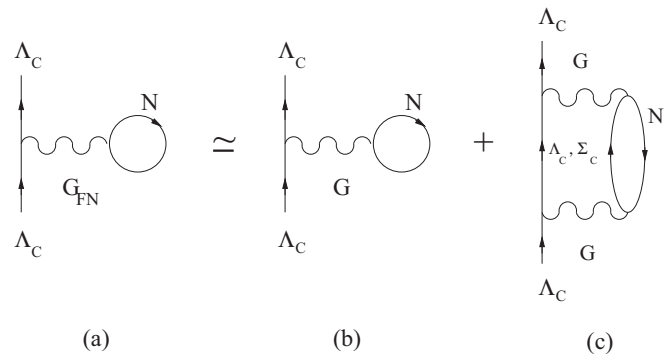

FIG. 4. Brueckner-Hartree-Fock approximation to the finite nucleus Λ_c self-energy (diagram a), split into the sum of a first-order contribution (diagram (b)) and a second-order 2p1h correction (diagram c).

in the finite nucleus is formally identical to Eq. (6), the only difference being the intermediate particle-particle propagator (i.e., Pauli operator and energy denominator), which corresponds to that in the finite nucleus. Alternatively, one can find the appropriate $G_{\rm FN}$ by relating it to the nuclear matter Y_cN G matrix already obtained. Eliminating the bare interaction V in both finite nucleus and nuclear matter Bethe-Goldstone equations it is not difficult to write $G_{\rm FN}$ in terms of G through the following integral equation:

$$\begin{aligned} G_{\rm FN} &= G + G\left[\left(\frac{Q}{E}\right)_{\rm FN} - \left(\frac{Q}{E}\right)\right] G_{\rm FN} \\ &= G + G\left[\left(\frac{Q}{E}\right)_{\rm FN} - \left(\frac{Q}{E}\right)\right] G \\ &\quad + G\left[\left(\frac{Q}{E}\right)_{\rm FN} - \left(\frac{Q}{E}\right)\right] G\left[\left(\frac{Q}{E}\right)_{\rm FN} - \left(\frac{Q}{E}\right)\right] G \\ &\quad + \cdots, \end{aligned} \quad (7)$$

which involves the nuclear matter G matrix and the difference between the finite nucleus and the nuclear matter propagators, written schematically as $(Q/E)_{\rm FN} - (Q/E)$. This difference, which accounts for the relevant intermediate particle-particle states, has been shown to be quite small (see Refs. [40–45]) and, therefore, in all practical calculations $G_{\rm FN}$ can be well approximated by truncating the expansion (7) up to second order in the nuclear matter G matrix. Therefore, we have

$$G_{\rm FN} \approx G + G\left[\left(\frac{Q}{E}\right)_{\rm FN} - \left(\frac{Q}{E}\right)\right] G. \quad (8)$$

The finite nucleus Λ_c self-energy can be obtained in the so-called Brueckner-Hartree-Fock approximation using the $G_{\rm FN}$ as an effective Y_cN interaction, as it is shown in diagram (a) of Fig. 4. According to Eq. (8) it can be split into the sum of the diagram (b), which represents the first-order term on the right-hand side of Eq. (8), and the diagram (c), which stands for the so-called two- particle-one-hole (2p1h), where the intermediate particle-particle propagator has to be viewed as the difference of propagators appearing in Eq. (8).

Schematically, it reads

$$\Sigma_{\rm BHF} = \sum_N \langle \Lambda_c N | G_{\rm FN} | \Lambda_c N \rangle \approx \sum_N \langle \Lambda_c N | G | \Lambda_c N \rangle + \sum_{Y_c N} \langle \Lambda_c N | G | Y_c N \rangle \times \left[\left(\frac{Q}{E} \right)_{\rm FN} - \left(\frac{Q}{E} \right) \right] \langle Y_c N | G | \Lambda_c N \rangle. \quad (9)$$

Detailed expressions for the first-order and the 2p1h contributions to $\Sigma_{\rm BHF}$ can be derived in close analogy to those for the finite nucleus Λ self-energy given in Refs. [42–45], being, in fact, formally identical. The interested reader is referred to these works for details on the derivation and for specific expressions of both contributions.

Finally, the self-energy can then be used as an effective Λ_c-nucleus mean-field potential in a Schrödinger equation to obtain the energies and wave functions of the bound states of the Λ_c in a finite nucleus. The Schrödinger equation is solved by diagonalizing the corresponding single-particle Hamiltonian (which includes also the Coulomb potential because the Λ_c is a positively charged baryon) in a complete basis within a spherical box of radius $R_{\rm box}$ following the procedure outlined in Refs. [40–45]. Although this method has been thoroughly described in these works, we repeat here some of the details.

The radius of the box should be larger than the radius of the nucleus considered. We note that the calculated observables are independent of the choice of $R_{\rm box}$ if this is chosen to be around 20 fm or larger. A complete and orthonormal set of regular basis functions within this box is given by

$$\Phi_{nljm}(\vec{r}) = \langle \vec{r} | k_n l j m \rangle = N_{nl}\, j_l(k_n r) \psi_{ljm}(\theta, \phi), \quad (10)$$

where N_{nl} is a normalization constant, $\psi_{ljm}(\theta, \phi)$ represents the spherical harmonics including the spin degrees of freedom, and $j_l(k_n r)$ denotes the spherical Bessel function for a momentum value k_n within the set of discrete momenta that fulfill the condition $j_l(k_n R_{\rm box}) = 0$. The single-particle Hamiltonian for the Λ_c charmed baryon can be evaluated in this basis and the resulting eigenvalue problem

$$\sum_{p=1}^{N_{\rm max}} \langle k_n | \frac{\hbar^2 k_n^2}{2M_{\Lambda_c}} \delta_{np} + \Sigma_{\rm BHF}(\omega = e_\gamma) + V_C | k_p \rangle \langle k_p | \gamma \rangle = e_\gamma \langle k_n | \gamma \rangle, \quad (11)$$

restricted typically to 20 or 30 states, can easily be solved. We note that a self-consistent procedure is required for each eigenvalue, i.e., the Λ_c self-energy should be evaluated at the energy of the resulting eigenvalue. As a result, one obtains the energies for the bound states and the corresponding wave functions, which are expressed in terms of the coefficients for the basis defined in Eq. (10).

IV. RESULTS

The energy of Λ_c single-particle bound states in ${}^{5}_{\Lambda_c}$He, ${}^{13}_{\Lambda_c}$C, ${}^{17}_{\Lambda_c}$O, ${}^{41}_{\Lambda_c}$Ca, ${}^{91}_{\Lambda_c}$Zr, and ${}^{209}_{\Lambda_c}$Pb are shown in Table III for the three models considered. For comparison the energy of the single-particle bound states of the Λ hyperon in the corresponding hypernuclei, obtained with the original Jülich $\tilde{A}$ YN interaction using the method described in the previous section, are also reported in Table III. Note that all charmed nuclei (hypernuclei) considered consist of a closed-shell nuclear core plus a Λ_c (Λ) sitting in a single-particle state. Model A gives the most attractive $\Lambda_c N$ interaction and, therefore, it predicts Λ_c single-particle states more bound than models B and C, and a larger number of them, as it can be seen in Table III. Note that, in the lack of experimental data on Λ_c nuclei, we cannot say *a priori* which one of the three models is better. However, since models B and C predict, as we saw before, scattering observables in better agreement with those extrapolated from LQCD in Ref. [38], it would not be too risky to state that these two models are probably more realistic than model A.

Looking now back at Table III we observe (as in the case of single Λ-hypernuclei) a small spin-orbit splitting of the p-, d-, and f-wave states in all Λ_c nuclei, especially in the case of the heavier ones where it is of the order of a few tenths of MeV. In addition, we also note that, since the Λ_c is heavier than the Λ, the level spacing of the Λ_c single-particle energies is, for the three models, always smaller than that for the corresponding hypernuclei. These observations are in agreement with the results previously obtained by Tsushima and Khanna in Refs. [31–33] using the quark-meson coupling model and, later, by Tan and Ning in Ref. [34] within a relativistic mean-field approach. Although there exist formal differences between our calculation and those of Refs. [31–34] that give rise to different predictions for the Λ_c single-particle bound states in finite nuclei, our results (particularly those for models B and C) are in general compatible with those of these works (see, e.g., Tables I and II of Ref. [31] and Table I of Ref. [34]).

We would like to note that if we used the bare $Y_c N$ interaction instead of the finite nucleus G matrix, i.e., if we worked in the Born approximation to obtain the Λ_c self-energy, then all the in-medium and correlation effects taken into account by the G matrix would be ignored and, as a result, due to the short-range repulsion of the bare $Y_c N$ interaction, much fewer bound states of the Λ_c would be found. As an illustration we show in Table IV the single-particle bound states of the Λ_c in ${}^{5}_{\Lambda_c}$He, ${}^{13}_{\Lambda_c}$C, and ${}^{17}_{\Lambda_c}$O obtained in this approximation. Results for the Λ hyperon in the corresponding Λ hypernulei are not shown because, in this case, no bound states are found when using this approximation. Note that model A is still able to predict (for the three nuclei) the same amount of bound states although all of them are shallower. This is not the case for models B and C for which the number of bound states is reduced (see Table III for comparison).

It has been pointed out in Refs. [31–34] and, more recently, also in Ref. [37] that the Coulomb interaction plays a non-negligible role in Λ_c nuclei, and that their existence is only possible if their binding energy is larger than the Coulomb repulsion between the Λ_c and the protons. To understand better the effect of the Coulomb force in our calculation, in Fig. 5 we explicitly show the contributions of the kinetic energy, the $Y_c N$ interaction, and the Coulomb potential to the energy of the Λ_c single-particle bound state $1s_{1/2}$ as functions of the mass number ($A = N + Z + 1$, with N being the neutron number and Z being the atomic number) of the Λ_c

TABLE III. Energy of Λ_c single-particle bound states of several charmed nuclei from ${}^{5}_{\Lambda_c}$He to ${}^{209}_{\Lambda_c}$Pb obtained for the three models considered. Results for the single-particle bound states of the Λ hyperon in the corresponding hypernuclei predicted by the original Jülich $\tilde{A}$ *YN* interaction are also shown for comparison. Units are given in MeV.

	${}^{5}_{\Lambda_c}$He			${}^{5}_{\Lambda}$He	${}^{13}_{\Lambda_c}$C			${}^{13}_{\Lambda}$C	${}^{17}_{\Lambda_c}$O			${}^{17}_{\Lambda}$O
	Model A	Model B	Model C	J$\tilde{A}$	Model A	Model B	Model C	J$\tilde{A}$	Model A	Model B	Model C	J$\tilde{A}$
$1s_{1/2}$	−13.58	−3.24	−1.05	−1.49	−27.26	−10.20	−5.47	−7.84	−31.76	−12.47	−6.96	−10.04
$1p_{3/2}$	−1.74	–	–	–	−14.91	−2.13	–	–	−19.99	−4.32	−0.51	−0.33
$1p_{1/2}$	−0.39	–	–	–	−13.42	−1.03	–	–	−18.79	−3.22	–	−0.35
$1d_{5/2}$	–	–	–	–	−4.10	–	–	–	−9.02	–	–	–
$1d_{3/2}$	–	–	–	–	−2.13	–	–	–	−6.96	–	–	–
$2s_{1/2}$	–	–	–	–	−3.59	–	–	–	−7.13	–	–	–
	${}^{41}_{\Lambda_c}$Ca			${}^{41}_{\Lambda}$Ca	${}^{91}_{\Lambda_c}$Zr			${}^{91}_{\Lambda}$Zr	${}^{209}_{\Lambda_c}$Pb			${}^{209}_{\Lambda}$Pb
	Model A	Model B	Model C	J$\tilde{A}$	Model A	Model B	Model C	J$\tilde{A}$	Model A	Model B	Model C	J$\tilde{A}$
$1s_{1/2}$	−41.09	−16.89	−9.60	−17.33	−44.76	−18.46	−10.51	−24.61	−52.52	−20.33	−10.32	−31.41
$1p_{3/2}$	−32.39	−10.41	−4.13	−7.67	−39.60	−14.27	−6.75	−17.66	−49.06	−18.28	−8.82	−27.59
$1p_{1/2}$	−31.60	−9.67	−3.42	−7.78	−39.24	−14.00	−6.49	−17.58	−48.84	−18.10	−8.64	−27.58
$1d_{5/2}$	−23.10	−3.91	–	–	−33.74	−9.63	−2.57	−9.12	−42.37	−12.94	−4.25	−19.24
$1d_{3/2}$	−21.84	−2.74	–	–	−33.17	−9.01	−1.95	−8.91	−41.97	−12.58	−3.88	−19.20
$1f_{7/2}$	−13.54	–	–	–	−27.06	−4.65	–	−1.35	−37.47	−9.11	−0.59	−10.51
$1f_{5/2}$	−11.82	–	–	–	−26.29	−3.80	–	−1.13	−37.07	−8.65	−0.10	−10.41
$2s_{1/2}$	−20.47	−2.74	–	–	−31.13	−8.05	−1.29	−6.60	−40.53	−10.20	−1.13	−17.43
$2p_{3/2}$	−10.20	–	–	–	−22.81	−2.23	–	−0.39	−39.21	−9.28	−0.03	−7.68
$2p_{1/2}$	−9.24	–	–	–	−22.24	−1.45	–	−0.38	−38.95	−9.06	–	−7.60
$2d_{5/2}$	−2.04	–	–	–	−14.62	–	–	–	−30.28	−5.36	–	−4.85
$2d_{3/2}$	−0.95	–	–	–	−14.03	–	–	–	−29.83	−4.75	–	−4.79
$2f_{7/2}$	–	–	–	–	−7.90	–	–	–	−22.57	–	–	–
$2f_{5/2}$	–	–	–	–	−6.81	–	–	–	−22.10	–	–	–
$3s_{1/2}$	−1.15	–	–	–	−13.41	–	–	–	−23.80	−1.51	–	−3.59
$3p_{3/2}$	–	–	–	–	−5.65	–	–	–	−22.32	–	–	–
$3p_{1/2}$	–	–	–	–	−5.61	–	–	–	−21.95	–	–	–
$3d_{5/2}$	–	–	–	–	–	–	–	–	−19.05	–	–	–
$3d_{3/2}$	–	–	–	–	–	–	–	–	−18.33	–	–	–
$3f_{7/2}$	–	–	–	–	–	–	–	–	−5.58	–	–	–
$3f_{5/2}$	–	–	–	–	–	–	–	–	−5.02	–	–	–
$4s_{1/2}$	–	–	–	–	–	–	–	–	−14.31	–	–	–
$4p_{3/2}$	–	–	–	–	–	–	–	–	−1.19	–	–	–
$4p_{1/2}$	–	–	–	–	–	–	–	–	−0.78	–	–	–
$4d_{5/2}$	–	–	–	–	–	–	–	–	−0.68	–	–	–
$5s_{1/2}$	–	–	–	–	–	–	–	–	−0.52	–	–	–

nuclei considered. Note that, while the Coulomb contribution increases because of the increase of the number of protons with the atomic number, those of the kinetic energy and the Y_cN interaction decrease when going from light to heavy Λ_c nuclei. The kinetic energy contribution decreases with the mass number because the wave function of the $1s_{1/2}$ state (see Fig. 6) becomes more and more spread due to the larger extension of the nuclear density over which the Λ_c wants to be distributed. The increase of the nuclear density with A leads to a more attractive Λ_c self-energy (see, e.g., Figs. 2 and 3 of Ref. [45] for a detailed discussion in the case of single Λ hypernuclei) that translates into a more negative contribution of the Y_cN interaction. Note that, when adding the three contributions, the energy of the $1s_{1/2}$ bound state decreases by several MeV in the low-mass-number region and then it tends to saturate for heavier nuclei. This is due to a compensation between the attraction of the Y_cN interaction and the repulsion of the Coulomb force. We note that this compensation leads, particularly in the case of model B, to values of the Λ_c single-particle bound-state energies similar

TABLE IV. Energy of Λ_c single-particle bound states of ${}^{5}_{\Lambda_c}$He, ${}^{13}_{\Lambda_c}$C, and ${}^{17}_{\Lambda_c}$O obtained in the Born approximation. Results for the Λ hyperon in the corresponding hypernuclei obtained with the bare Jülich $\tilde{A}$ YN interaction are not shown because, in this case, no bound states are found in this approximation. Units are given in MeV.

	${}^{5}_{\Lambda_c}$He			${}^{13}_{\Lambda_c}$C			${}^{17}_{\Lambda_c}$O		
	Model A	Model B	Model C	Model A	Model B	Model C	Model A	Model B	Model C
$1s_{1/2}$	−9.48	−1.36	–	−21.81	−6.53	−2.24	−25.71	−8.15	−3.04
$1p_{3/2}$	−1.17	–	–	−10.39	–	–	−14.63	−1.29	–
$1p_{1/2}$	–	–	–	−8.68	–	–	−13.23	−0.09	–
$1d_{5/2}$	–	–	–	−0.96	–	–	−4.81	–	–
$1d_{3/2}$	–	–	–	–	–	–	−2.60	–	–
$2s_{1/2}$	–	–	–	−1.22	–	–	−3.74	–	–

to those obtained for single Λ hypernuclei with the Jülich $\tilde{A}$ YN potential (see Table III). We want to point out that even the less attractive one of our Y_cN interactions (model C), despite the Coulomb repulsion, is able to bind the Λ_c in all the nuclei considered. This is in contrast with the recent results of the HAL QCD Collaboration [37], which suggest that only light- or medium-mass Λ_c nuclei could really exist. However, we note that this conclusion is based on results obtained for a value of the pion mass of 410 MeV, giving rise to a Y_cN interaction much less attractive than ours and the one derived in Ref. [38] when these lattice results are extrapolated to the physical pion mass (see Figs. 1 and 2 of Ref. [38]).

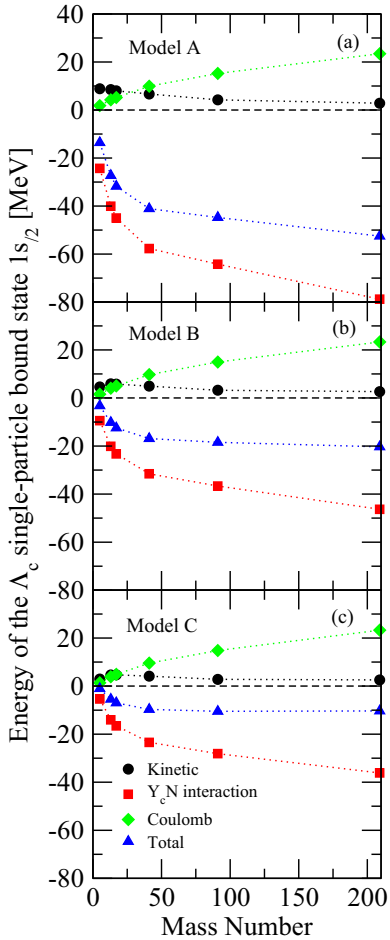

FIG. 5. Contributions of the kinetic energy, the Y_cN interaction, and the Coulomb potential to the energy of the Λ_c single-particle bound state $1s_{1/2}$ as a function of the mass number of the Λ_c nuclei considered.

Now we would like to focus the attention of the reader on the effect of the coupling of the Λ_cN and Σ_cN channels. These two channels are located at approximately 3224 and 3394 MeV, respectively. Being separated by about 170 MeV it is expected, as it was already pointed out by Tsushima and Khanna (see, e.g., Refs. [31,32]), that the effect of their coupling on charmed nuclei will be less important than that of the ΛN and ΣN channels (separated only by ∼80 MeV) on hypernuclei. This is illustrated in Table V, where we show as an example the energy of the Λ_c (Λ) single-particle states bound states of ${}^{17}_{\Lambda_c}$O (${}^{17}_{\Lambda}$O) when the Λ_cN-Σ_cN (ΛN-ΣN) coupling is switched off. Note that the differences between the levels obtained with the complete coupled-channel calculation for ${}^{17}_{\Lambda_c}$O (see Table III) and without the Λ_cN-Σ_cN coupling are almost negligible, being of the order of a few tenths of MeV or less, whereas those for ${}^{17}_{\Lambda}$O are slightly larger than 1 MeV. Note also that the elimination of the coupling between the Λ_cN and Σ_cN channels leads, in the case of models B and C, to a bit more of attraction, contrary to what happens in hypernuclei, for which the Λ bound states become less bound when the ΛN-ΣN coupling is eliminated.

TABLE V. Energy of Λ_c single-particle bound states of ${}^{17}_{\Lambda_c}$O when the coupling of the Λ_cN and the Σ_cN channels is switched off. Results for the Λ hyperon in ${}^{17}_{\Lambda}$O obtained with the original Jülich $\tilde{A}$ YN interaction are also shown for comparison. Units are given in MeV.

	Model A	Model B	Model C	J$\tilde{A}$
$1s_{1/2}$	−31.54	−12.57	−7.11	−8.78
$1p_{3/2}$	−19.69	−4.37	−0.58	–
$1p_{1/2}$	−18.45	−3.24	–	–
$1d_{5/2}$	−8.71	–	–	–
$1d_{3/2}$	−6.62	–	–	–
$2s_{1/2}$	−7.02	–	–	–

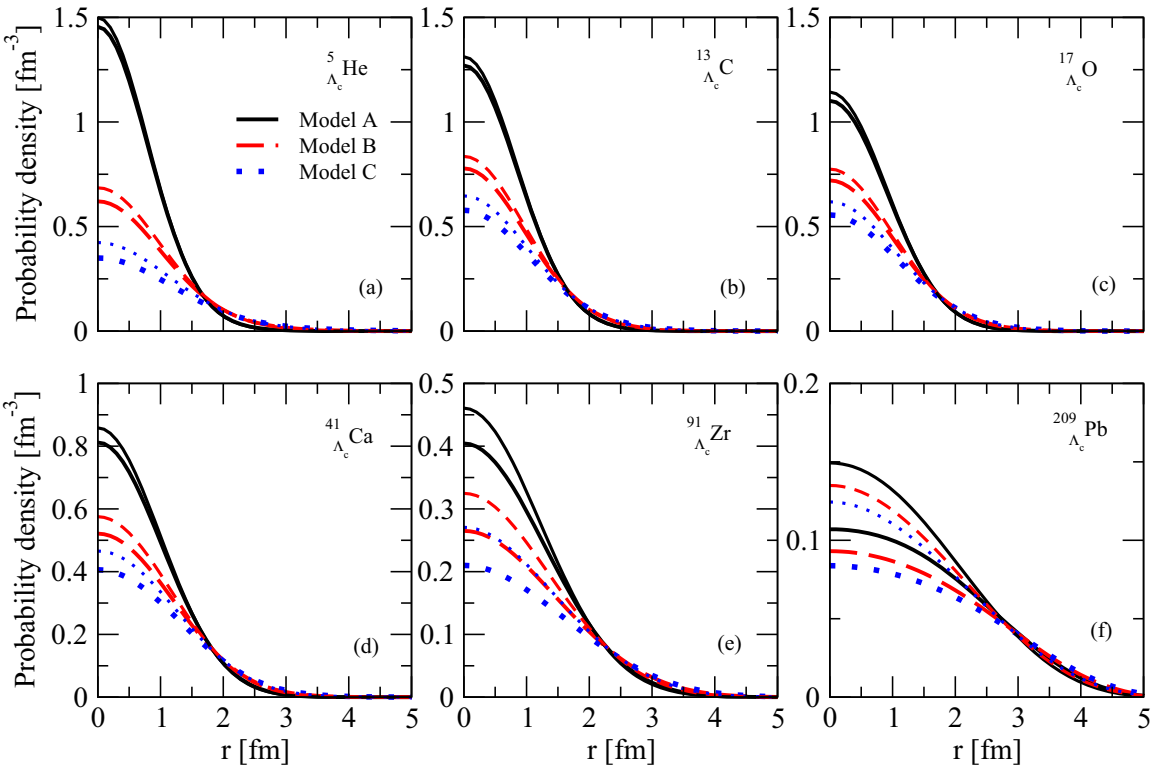

FIG. 6. Λ_c probability density distribution for the $1s_{1/2}$ state in the six Λ_c nuclei considered. Results are shown for the three models A, B, and C of the Y_cN interaction. Thin solid, dashed, and dotted lines show the results when the Coulomb interaction is artificially switched off.

We finish this section by showing in Fig. 6, for the three models, the probability density distribution (i.e., the square of the radial wave function) of the Λ_c in the $1s_{1/2}$ state for the six Λ_c nuclei considered. The result when the Coulomb interaction is artificially switched off is also shown for comparison (thin solid, dashed, and dotted lines). Note that, due to the increase of the nuclear density, when moving from light to heavy nuclei the probability density of finding the Λ_c close to the center of the nucleus decreases, and it becomes more and more distributed over the whole nucleus. Note also that, as expected, the Coulomb repulsion pushes the Λ_c away from the center of the nuclei. A similar discussion can be done for the probability densities of the other Λ_c single-particle bound states.

V. SUMMARY AND CONCLUSIONS

In this work we have determined the single-particle energies of the Λ_c charmed baryon in several nuclei. To such end, we have developed a charmed baryon-nucleon interaction based on a SU(4) extension of the meson-exchange hyperon-nucleon potential $\tilde{A}$ of the Jülich group. We have considered three different models of this interaction (A, B, and C) that differ only in the values of the couplings of the scalar σ meson with the charmed baryons. Several scattering observables have been computed with the three models and compared with those predicted by the Y_cN interaction derived by Haidenbauer and Krein [38] from the extrapolation to the physical pion mass of the recent results of the HAL QCD Collaboration [37]. Qualitative agreement has been found between the predictions of our models B and C and those of the model by Haidenbauer and Krein [38].

The three models have then been used to obtain the self-energy of the Λ_c in finite nuclei by using a many-body approach that started with the construction of a nuclear matter Y_cN G matrix from which a finite nucleus one was derived through a perturbative expansion. Using the resulting Λ_c self-energy as an effective Λ_c-nucleus mean-field potential in a Schrödinger equation we have finally obtained the energies and wave functions of the bound states of the Λ_c in the different nuclei.

Our results (particularly those for models B and C) are compatible with those obtained by Tsushima and Khanna [31–33] and Tan and Ning [34], despite the formal differences between our calculation and those of these works based, respectively, on the quark-meson coupling model and the relativistic mean-field approach. A small spin-orbit splitting of the p-, d-, and f-wave states has been found as in the case of single Λ hypernuclei. It has been also observed that level spacing of the Λ_c single-particle energies is smaller than the corresponding one for hypernuclei.

We have analyzed the role played by the Coulomb potential in the energies of the Λ_c single-particle bound states. This analysis has shown that the compensation between the Y_cN interaction and the repulsion of the Coulomb force leads, particularly in the case of model B, to values of the Λ_c single-particle bound-state energies similar to those obtained for the single Λ-hypernuclei with the original Jülich $\tilde{A}$ YN

potential. The analysis has also shown that, despite the Coulomb repulsion, even the less attractive one of our Y_cN interactions (model C) is able to bind the Λ_c in all the nuclei considered. This is in contrast with the recent results of the HAL QCD Collaboration [37] which suggest that only light- or medium-mass Λ_c nuclei could really exist. However, the conclusion of this work is based on results obtained for a value of the pion mass of 410 MeV, giving rise to a Y_cN interaction much less attractive than ours and the one derived in Ref. [38] when these lattice results are extrapolated to the physical pion mass.

Finally, we have shown that the effect of the coupling of the Λ_cN and Σ_cN channels on the single-particle properties of charmed nuclei is much less important (being in fact almost negligible) than that of the ΛN and ΣN channels on the corresponding properties of single Λ hypernuclei, due to the large mass difference of the Λ_c and Σ_c baryons of $\sim$170 MeV.

ACKNOWLEDGMENTS

The authors are very grateful to Johann Haidenbauer for his useful comments. This work has been partly supported by the COST Action CA16214, by the Spanish Ministerio de Economia y Competitividad (MINECO) under Project No. MDM-2014-0369 of ICCUB (Unidad de Excelencia "María de Maeztu") and, with additional European FEDER funds, under Project No. FIS2017-87534-P, and by the Barcelona Center for Subsurface Imaging, Research Group 2017 SGR 1662 (Generalitat de Catalunya).

[1] C. L. Aubert *et al.*, Phys. Rev. Lett. **33**, 1404 (1974).
[2] J. Augustin *et al.*, Phys. Rev. Lett. **33**, 1406 (1974).
[3] E. G. Cazzoli *et al.*, Phys. Rev. Lett. **34**, 1125 (1975).
[4] G. Goldhaber *et al.*, Phys. Rev. Lett. **37**, 255 (1976).
[5] I. Peruzzi *et al.*, Phys. Rev. Lett. **37**, 569 (1976).
[6] B. Knapp, *et al.*, Phys. Rev. Lett. **37**, 882 (1976).
[7] A. A. Tyapkin, Yad. Fiz. **22**, 181 (1975); Sov. J. Nucl. Phys. **22**, 89 (1976).
[8] C. B. Dover and S. H. Kahana, Phys. Rev. Lett. **39**, 1506 (1977).
[9] C. B. Dover, S. H. Kahana, and T. L. Trueman, Phys. Rev. D **16**, 799 (1977).
[10] S. Iwao, Lett. Nuovo Cimento **19**, 647 (1977).
[11] R. Gatto and F. Paccanoni, Nuovo Cimento A **46**, 313 (1978).
[12] G. Bhamathi, Phys. Rev. C **24**, 1816 (1981).
[13] N. N. Kolesnikov *et al.*, Sov. J. Nucl. Phys. **34**, 957 (1981).
[14] H. Bandō and M. Bando, Phys. Lett. B **109**, 164 (1982).
[15] H. Bandō and S. Nagata, Prog. Theor. Phys. **69**, 557 (1983).
[16] H. Bandō, Prog. Theor. Phys. Suppl. **81**, 197 (1985).
[17] B. F. Gibson, C. B. Dover, G. Bhamathi, and D. R. Lehman, Phys. Rev. C **27**, 2085 (1983).
[18] G. Bhamathi, Nuovo Cimento A **102**, 607 (1989).
[19] T. Bressani and F. Iazzi, Nuovo Cimento A **102**, 597 (1989).
[20] S. A. Bunyatov, V. V. Lyukov, N. I. Starkov, and V. A. Tsarev, Nuovo Cimento A **104**, 1361 (1991).
[21] Y. A. Batusov *et al.*, JINR Preprint E1-10069 (Dubna 1976).
[22] Y. A. Batusov *et al.*, Pis'ma Zh. Eksp. Teor. Fiz. **33**, 56 (1981).
[23] Y. A. Batusov *et al.*, JETP Lett. **33**, 56 (1981).
[24] Y. A. Batusov *et al.*, JINR Communication P1-85-495 (Dubna 1985).
[25] V. V. Lyukov, Nuovo Cimento A **102**, 583 (1989).
[26] J. Riedl, A. Schäfer, and M. Stratmann, Eur. Phys. J. C **52**, 987 (2007); http://www.gsi.de/fair; http://j-parc.jp/index-e.html
[27] E. Tomasi-Gustafsson (PANDA Collaboration), Hyperfine Interact. **239**, 30 (2018).
[28] R. Shyam and K. Tsushima, Phys. Lett. B **770**, 236 (2017).
[29] G. Krein, A. W. Thomas, and K. Tsushima, Prog. Part. Nucl. Phys. **100**, 161 (2018).
[30] K. Tsushima and F. C. Khanna, Phys. Lett. B **552**, 138 (2003).
[31] K. Tsushima and F. C. Khanna, Prog. Theor. Phys. Suppl. **149**, 160 (2003).
[32] K. Tsushima and F. C. Khanna, Phys. Rev. C **67**, 015211 (2003).
[33] K. Tsushima and F. C. Khanna, J. Phys. G **30**, 1765 (2004).
[34] Y.-H. Tan and P.-Z. Ning, Europhys. Lett. **67**, 355 (2004).
[35] Y.-R. Liu and M. Oka, Phys. Rev. D **85**, 014015 (2012).
[36] S. Maeda, M. Oka, A. Yokota, E. Hiyama, and Y. R. Liu, Prog. Theor. Exp. Phys. **2016**, 023D02 (2016).
[37] T. Miyamoto *et al.*, Nucl. Phys. A **971**, 113 (2018).
[38] J. Haidenbauer and G. Krein, Eur. Phys. J. A **54**, 199 (2018).
[39] A. Reuber, K. Holinde, and J. Speth, Nucl. Phys. A **570**, 543 (1994).
[40] M. Borromeo, D. Bonatsos, H. Müther, and A. Polls, Nucl. Phys. A **539**, 189 (1992).
[41] M. Hjorth–Jensen, H. Müther, and A. Polls, Phys. Rev. C **50**, 501 (1994).
[42] M. Hjorth-Jensen, A. Polls, A. Ramos, and H. Müther, Nucl. Phys. A **605**, 458 (1996).
[43] I. Vidaña, A. Polls, A. Ramos, and M. Hjorth-Jensen, Nucl. Phys. A **644**, 201 (1998).
[44] I. Vidaña, Ph.D. thesis, University of Barcelona, 2001, http://www.tesisenxarxa.net/TDX-0709102-133910/
[45] I. Vidaña, Nucl. Phys. A **958**, 48 (2017).
[46] E. M. Haacke, J. W. Moffat, and P. Savaria, J. Math. Phys. **17**, 2041 (1976).
[47] J. Hao, T. T. S. Kuo, A. Reuber, K. Holinde, J. Speth, and D. J. Millener, Phys. Rev. Lett. **71**, 1498 (1993).
[48] D. Halderson, Phys. Rev. C **48**, 581 (1993).